Journal of Sound and Vibration (2002) **249**(1), 165–187
doi:10.1006/jsvi.2001.3857, available online at http://www.idealibrary.com on IDEAL®

RESONANT PROPERTIES OF SHORT EXPANSION CHAMBERS IN A CIRCULAR DUCT: INCLUDING EXTREMELY SHORT CASES AND ASYMMETRIC MODE WAVE INCIDENCE CASES

A. Sadamoto and Y. Murakami

Department of Mechanical Engineering, Tsukuba College of Technology, 4-3 *Amakubo*, *Tsukuba*, *Ibaraki*, 305-0005, *Japan. Email*: *sada@a.tsukuba-tech.ac.jp*

(*Received* 1 *March* 2001, *and in final form* 12 *July* 2001)

Resonant properties of short expansion chambers are studied comprehensively using a traditional analytical approach with simply refined equations. Containing enough number of radial modes in calculation, properties of chambers including the cases of extremely short ones and/or asymmetric mode waves incidence are investigated, and confirmed experimentally with the well-designed apparatus. For various dimensions of chambers and for any mode wave incidence, resonant properties are simply summarized using the resonant frequency, which is almost decisively normalized by the chamber depth and the wavelength of the plane wave for an extremely short one; and by the chamber diameter for a relatively long one with the transition length from acoustically short (resonant-type) to long (common-type): the length is also decided by the chamber diameter. As the case may be, the extremely short chamber might be applicable as a compact resonator muffler.

1. INTRODUCTION

Acoustic performance of an expansion chamber in a duct as a sound attenuator is well known. It is represented by the repeating dome-shaped transmission loss curve, in the case that the plane wave theory can be applied. But when the axial length of the chamber considerably shortens, this property changes remarkably and the chamber begins to act as a resonator muffler [1].

Assuming a circular expansion chamber concentric with a circular infinite duct and no duct extension in the chamber, this simple duct system is specified by the duct diameter D, the chamber diameter d and the chamber length l. When the ratio d/D and l/d are fixed, linear acoustic fields in the duct and the chamber can be described decisively with the relative frequency, regardless of the actual size of the duct system. Recently, Selamet *et al.* investigated the effect of the l/d ratio on the acoustic performance of concentric chambers experimentally and theoretically [2]. Although they were concerned with the wide range of the l/d ratio, they did not give a detailed description about resonant-type chambers of $l/d < 0{\cdot}41$: this important value corresponds to the transition chamber length from acoustically long to short [3]. In addition, they fixed the d/D ratio for one value as $d/D = 3{\cdot}15$. Especially in the range of $l/d < 0{\cdot}2$, they and other researchers [4] gave no description. Such a short chamber can be found in the report of Kuznetsov *et al.* [5], but they gave only few notations.

0022-460X/02/010165 + 23 $35.00/0

In these past several years, Selamet *et al.* have continuously and extensively published many results investigated with many types of expansion chambers in this journal [6]. On the other hand, in the 1990s, we independently have studied properties of concentric expansion chambers; developed the experimental apparatus and the calculation method; and mentioned the importance of decaying higher order modes excited at both discontinuities of the chamber's inlet and outlet as the same interpretation as that of Selamet *et al.* Different from Selamet *et al.*, however, we were especially interested in cases in which the l/d ratio is further small. Even in extremely small l/d ratio cases, we clarified that the property of the chamber could be calculated accurately using a traditional analytical approach [7], if enough number of higher order modes was taken into consideration for calculation.

For the practical noise reduction problem, e.g., exhaust noise of internal combustion engines of which dominant acoustic power is involved in a low-frequency range [8]; a short chamber is not generally used as a resonator muffler. Therefore, such a short chamber might have been out of interest for former and current researchers. But if an extremely short chamber works as a resonator, it would be expected to work as a compact muffler (which can be put in an axially small space), which is applicable to machines or ducting systems radiating monotonic and relatively high-frequency noise. Recently, such noise might create more serious problems because the size of recent machinery tends to become smaller; their driving speed tends to become higher; and some of the traditional low-frequency noise problems have been well treated now.

For practical reasons, many theoretical studies for circular duct systems have been limited to deal with only circularly symmetric modes. In some cases, however, asymmetric modes would cause serious duct noise, e.g., noise radiated from a jet engine [9]. It is easy to expand two-dimensional analytical equations to the cases of asymmetric modes incident to the chamber. We have demonstrated the accuracy of this expansion of analysis with the apparatus that can radiate asymmetric modes propagating in a duct.

Our research concerning some matters mentioned above had been already completed. Some of these results [10–12] are reviewed in this paper in order to clarify our method of calculation and experiment. The main results newly obtained in this paper are presented in section 5 as the relation between resonant frequencies and dimensions of resonant-type chambers with various l/d and d/D ratios, including the cases of asymmetric modes incidence.

2. THEORETICAL CALCULATION METHOD

In this study, we consider an expansion chamber as shown in Figure 1. To treat it as a distributed-parameter system, sound behavior at a discontinuity in a duct must be described first. For this purpose, we follow Miles and Alfredson's calculation methods [7, 13]. By adding some modifications to their descriptions, the sound pressure in a hard-walled circular duct is written as

$$p = \sum_{m=0}^{\infty} \sum_{n=0}^{\infty} P_{mn} \mathbf{J}_m \left(\frac{\omega_{mn} r}{c} \right) \cos(m\theta) \exp \left\{ \mathrm{j}\omega \left(t \pm \frac{z}{v_{mn}} \right) \right\} \tag{1}$$

with the cylindrical co-ordinate (r, θ, z), where r, θ and z indicates the radial, circumferential and axial direction respectively.

Equation (1) is realized as the superposition of each (m, n) mode wave with angular frequency ω, where m and n are integers, which, respectively, refer to the circumfernetial and radial order of each mode wave. For reference, some mode shapes are shown in Figure 2,

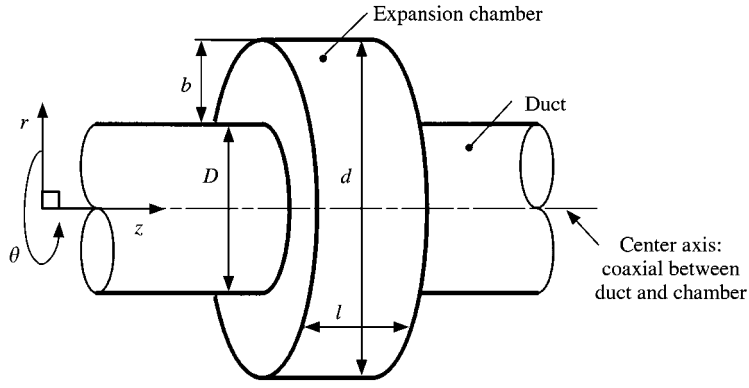

Figure 1. An expansion chamber.

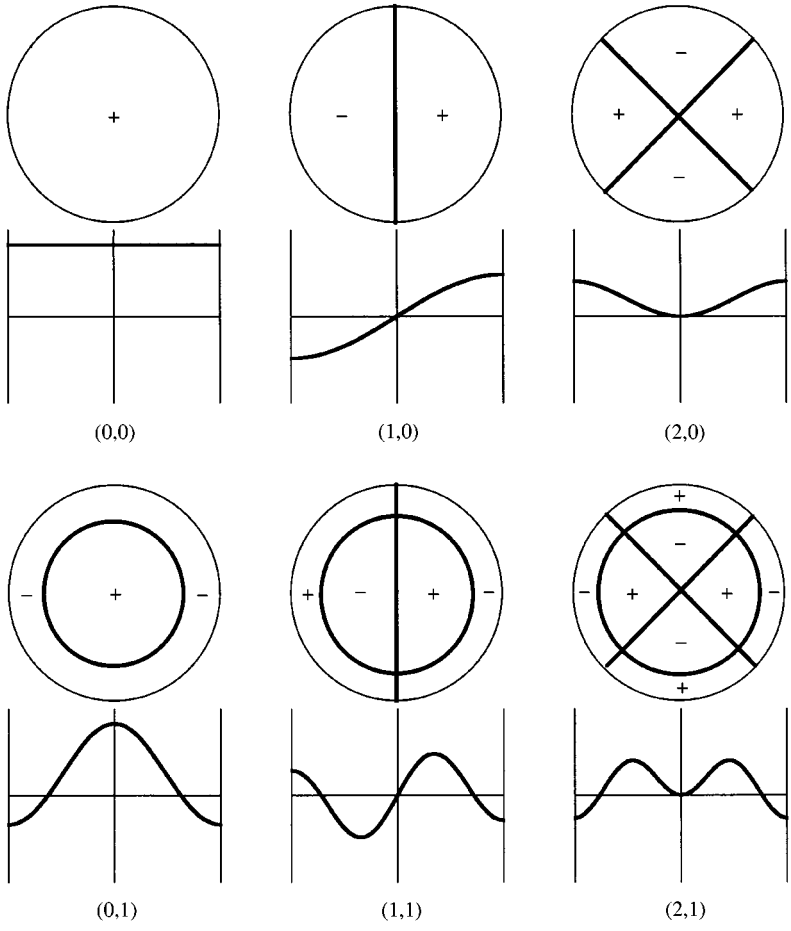

Figure 2. Shapes of the (m, n) mode waves.

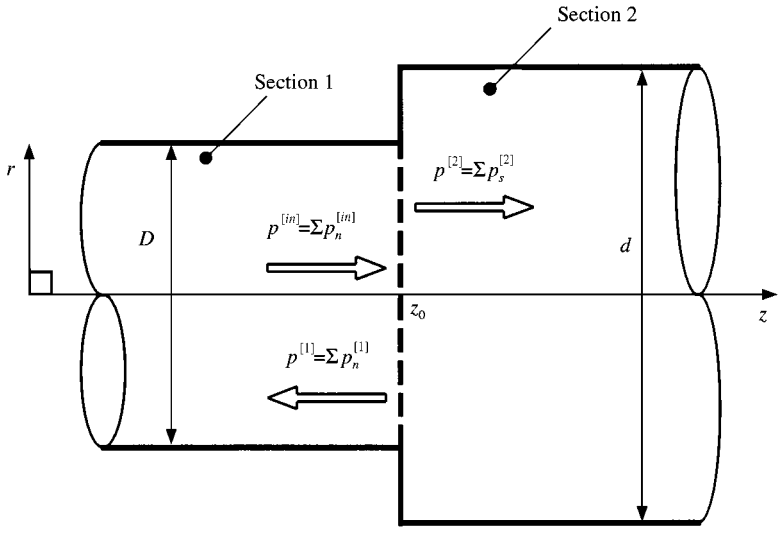

Figure 3. A discontinuity in a duct.

where each outer circle indicates the duct wall; the solid lines in each circle indicate the nodes of each mode; and the radial distribution of the sound pressure of each mode is indicated below each circle. Formerly, we had regarded (m, n) as $(m, n + 1)$ except the symmetric $(m = 0)$ modes. Namely, we labelled (1, 1) instead of (1, 0), (2, 1) instead of (2, 0), and so on. This labelling rule might be reasonable when one's attention was directed not to the number of nodal circles but to the sound pressure distribution through the diameter shown in Figure 2. In this paper, however, we follow the general notation rule of higher order modes [14].

In equation (1), P_{mn} is a complex number that indicates the amplitude and phase in the z direction of the (m, n) mode wave. J_m is the Bessel function of the first kind of order m. c is the sound velocity in free space, ω_{mn} is the cut-off angular frequency of the (m, n) mode wave. It equals $2q_{mn}c/D$ that is given by the boundary condition at the rigid wall of the duct with diameter D, where q_{mn} is the value of root for $dJ_m/dq = 0$: in the range of $q > 0$, the nth root for $m = 0$; and the $(n + 1)$th root for $m \geqslant 1$. v_{mn} is the phase velocity in the z direction of the (m, n) mode wave, and is given by $c\omega(\omega^2 - \omega_{mn}^2)^{-1/2}$. If $\omega < \omega_{mn}$, v_{mn} becomes imaginary, and the corresponding (m, n) mode wave cannot propagate in the duct. Generally, the wavenumber k_{zmn} $(= \omega/v_{mn})$ in the z direction and k_{rmn} $(= \omega_{mn}/c)$ in the r direction are used in equation (1), but we use v_{mn} and ω_{mn}, because whichever parameters are used, there is no difference in terms of simplicity in the following equations.

We consider a discontinuity in a duct as shown in Figure 3. The hard-walled duct with infinite length in the z direction is separated into two sections at the discontinuity as sections 1 and 2, corresponding to the duct and the chamber, respectively, in the later part of this chapter. In the process of arranging equations, we try to simplify the notation as much as possible in order to write a brief program code of computational calculation. For this reason, some rules are made as follows:

(1) The ratio of each section's diameter is defined as

$$R_d = d/D, \tag{2}$$

that always follows the condition $d > D$, i.e., $R_d > 1$.

(2) Because both sections are concentric, the circumferential mode (m) of any incident wave at the discontinuity does not change when it reflects and transmits. In the following, hence, the notation m is eliminated, because each m is mutually independent for the calculation. For example, ω_{mn} is denoted as ω_n.

(3) The suffix$^{[1]}$ is used for section 1, and $^{[2]}$ for section 2. For example, the cut-off angular frequency in section 1 is denoted as $\omega_n^{[1]}$.

(4) For the numerical calculation, the upper limit of n must be decided. With reference to Hudde's research [15], in order to give the same order contributions of radial modes in each section, the upper value of n is determined as an arbitrary integer following the conditions:

$$n_2/n_1 \approx R_d, \quad \text{for } m = 0;$$
$$(n_2 + 1)/(n_1 + 1) \approx R_d, \quad \text{for } m \geqslant 1, \tag{3}$$

where n_1 is for section 1, and n_2 is for section 2.

(5) The symbols n and u are used in order to indicate the radial mode number for section 1, and s for section 2.

If the incident wave ($p^{[in]}$ in Figure 3) propagates in section 1 toward section 2, the discontinuity becomes an abrupt expansion. In this case, the reflected wave ($p^{[1]}$) in section 1 and the transmitted wave ($p^{[2]}$) in section 2 are radiated at the discontinuity, but the wave propagating in the negative z direction in section 2 does not exist, because the duct has infinite length. The sound pressures, which should be considered in Figure 3, are the following:

$$p^{[in]} = \sum_{n=0}^{n_1} P_n \mathrm{J}_m\left(\frac{\omega_n^{[1]} r}{c}\right) \cos m\theta \exp\left\{\mathrm{j}\omega\left(t - \frac{z}{v_n^{[1]}}\right)\right\}, \tag{4}$$

$$p^{[1]} = \sum_{n=0}^{n_1} P_n^{[1]} \mathrm{J}_m\left(\frac{\omega_n^{[1]} r}{c}\right) \cos m\theta \exp\left\{\mathrm{j}\omega\left(t + \frac{z - z_0}{v_n^{[1]}}\right)\right\} \tag{5}$$

and

$$p^{[2]} = \sum_{s=0}^{n_2} P_s^{[2]} \mathrm{J}_m\left(\frac{\omega_s^{[2]} r}{c}\right) \cos m\theta \exp\left\{\mathrm{j}\omega\left(t - \frac{z - z_0}{v_s^{[2]}}\right)\right\}. \tag{6}$$

The relation among them can be solved using the boundary conditions at the discontinuity: (1), continuity of the sound pressure and the axial velocity over the region $0 \leqslant r \leqslant D/2$; and (2), zero axial velocity in section 2 over the region $D/2 \leqslant r \leqslant d/2$. A disregard of the sound pressure over the region $D/2 \leqslant r \leqslant d/2$ is not a serious matter in this research as confirmed experimentally in section 3.

In order to calculate the reflection and transmission coefficients at the discontinuity, we denote the complex amplitude of the incident wave of order n at $z = z_0$ as $P_n^{[in]}$ $[= P_n \exp(-\mathrm{j}\omega z_0/v_n^{[1]})]$. Using the orthogonal relations of Bessel functions, the equations relating $P_n^{[in]}$, $P_n^{[1]}$ and $P_s^{[2]}$, which are independent for t and θ, can be arranged as

$$P_u^{[1]} = -P_u^{[in]} + \frac{1}{K_1(u)} \sum_{s=0}^{n_2} K_2(u, s) P_s^{[2]} \quad (u = 0, 1, \ldots, n_1) \tag{7}$$

and

$$P_s^{[2]} = \frac{v_s^{[2]}}{K_4(u)} \sum_{n=0}^{n_1} \left\{\frac{K_3(n, s)}{v_n^{[1]}} (P_n^{[in]} - P_n^{[1]})\right\} \quad (s = 0, 1, \ldots, n_2), \tag{8}$$

where K_1, K_2, K_3 and K_4 are given as follows:

$$K_1(u) = \begin{cases} 1 & \text{for } m = u = 0 \quad \text{corresponding to the plane wave,} \\ \{1 - (n/q_u)^2\}\, \mathrm{J}_m(q_u), & \text{for other cases,} \end{cases} \tag{9, 10}$$

$$K_2(u, s) = \begin{cases} K_1(u) & \text{for the cases of } \omega_u^{[1]} = \omega_s^{[2]}, \\ \{2R_d q_s \mathrm{J}'_m(q_s/R_d)\}/\{(R_d q_u)^2 - q_s^2\} & \text{for } \omega_u^{[1]} \neq \omega_s^{[2]}, \end{cases} \tag{11, 12}$$

$$K_3(n, s) = \begin{cases} 1 & \text{for } m = n = 0, \\ \{1 - (n/q_n)^2\}\, \{\mathrm{J}_m(q_n)\}^2 & \text{for } \omega_n^{[1]} = \omega_s^{[2]} \text{ except the upper case,} \\ \{2R_d q_s \mathrm{J}_m(q_n)\mathrm{J}'_m(q_s/R_d)\}/\{(R_d q_n)^2 - q_s^2\} & \text{for } \omega_n^{[1]} \neq \omega_s^{[2]}, \end{cases} \tag{13, 14, 15}$$

$$K_4(s) = \begin{cases} R_d^2 & \text{for } m = s = 0, \\ \{1 - (n/q_s)^2\}\, \{R_d \mathrm{J}_m(q_s)\}^2 & \text{for other cases.} \end{cases} \tag{16, 17}$$

In equations (11), (12), (14) and (15), K_2 and K_3 are distributed for the values of $\omega_n^{[1]}$ and $\omega_s^{[2]}$. Miles and Alfredson, and other researchers who followed them [1, 2], did not refer to this distribution, but this is necessary to prevent the denominator of the right-hand side of equations (12) and (15) from becoming zero.From the viewpoint of numerical calculation, an error occur when a denominator takes on a value close to 0. In our calculation program, equations (11) and (14) are used, when $\omega_n^{[1]}$ is close to $\omega_s^{[2]}$ in an arbitrary range.

By eliminating $P_s^{[2]}$ using equations (7) and (8), simultaneous equations are conducted:

$$\sum_{n=0}^{n_1} A_{un} P_n^{[1]} = \sum_{n=0}^{n_1} B_{un} P_n^{[in]} \quad (u = 0, 1, \ldots, n_1), \tag{18}$$

where

$$A_{un} = \sum_{s=0}^{n_2} \frac{K_2(u, s) K_3(n, s)}{K_4(s)} \frac{v_s^{[2]}}{v_n^{[1]}} + \delta_{un} K_1(u) \quad (u = 0, 1, \ldots, n_1), \tag{19}$$

$$B_{un} = \sum_{s=0}^{n_2} \frac{K_2(u, s) K_3(n, s)}{K_4(s)} \frac{v_s^{[2]}}{v_n^{[1]}} - \delta_{un} K_1(u) \quad (u = 0, 1, \ldots, n_1), \tag{20}$$

where δ_{un} is Kronecker's δ. By solving equation (18) with arbitrary values of $P_n^{[in]}$ ($n = 0$, $1, \ldots, n_1$), the reflected wave's complex amplitudes $P_n^{[1]}$ ($n = 0, 1, \ldots, n_1$) are obtained. Then, by substituting these values of $P_n^{[1]}$ for equation (8), the transmitted wave's complex amplitudes $P_s^{[2]}$ ($s = 0, 1, \ldots, n_2$) are obtained.

If the incident wave propagates in section 2 toward section 1 in Figure 3, the discontinuity becomes an abrupt reduction. In this case, the reflected wave in section 2 and the transmitted wave in section 1 are radiated at the discontinuity. Sound pressures of each wave are denoted by equations (5) and (6), but equation (4) must be replaced by

$$p^{[in]} = \sum_{s=0}^{n_2} P_s \mathrm{J}_m\left(\frac{\omega_s^{[2]} r}{c}\right) \cos m\theta \exp\left\{\mathrm{j}\omega\left(t + \frac{z}{v_s^{[2]}}\right)\right\} \tag{21}$$

and the complex amplitude of the incident wave of order s at $z = z_0$ is replaced by $P_s^{[in]}$ [$= P_s \exp(\mathrm{j}\omega z_0/v_s^{[2]})$]. Using almost the same process mentioned above, simultaneous

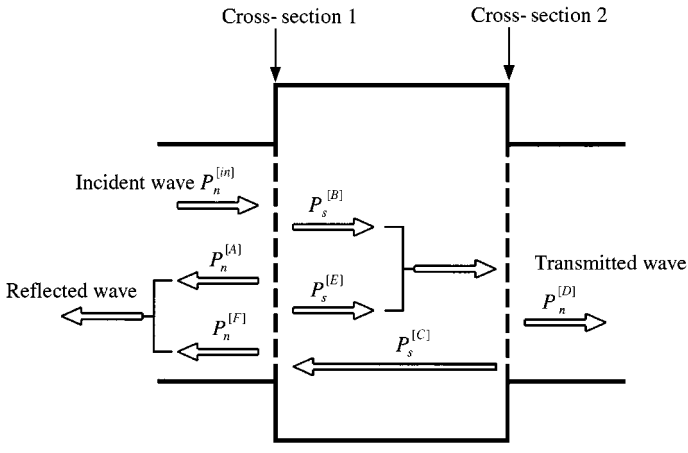

Figure 4. Outline of calculation of chamber's property.

equations are conducted as

$$\sum_{n=0}^{n_1} A_{un} P_n^{[1]} = 2 \sum_{s=0}^{n_2} K_2(u, s)\ P_s^{[in]} \quad (u = 0, 1, \ldots, n_1) \tag{22}$$

and $P_n^{[1]}$ $(n = 0, 1, \ldots, n_1)$ are obtained by solving them. Then, $P_s^{[2]}$ $(s = 0, 1, \ldots, n_2)$ are obtained by substituting these $P_n^{[1]}$ into

$$P_s^{[2]} = P_s^{[in]} - \frac{v_s^{[2]}}{K_4(s)} \sum_{n=0}^{n_1} \left\{ \frac{K_3(n, s)}{v_n^{[1]}} P_n^{[in]} \right\} \quad (s = 0, 1, \ldots, n_2). \tag{23}$$

In the procedure for calculating equations (22) and (23), the values of A_{un}, K_1, K_2, K_3 and K_4 have already been calculated in equations (9)–(17) and (19). In the calculation procedure for an expansion chamber mentioned below, it is not necessary to re-calculate these values in one program code.

On the basis of the above equations, we calculate sound properties of an expansion chamber shown in Figure 1. Our method explained below with Figure 4 is similar to Alfredson's one [13]. It is supposed that the incident wave from the left side of the duct has one circumferential mode m and several radial modes n with the complex amplitudes $P_n^{[in]}$. It is not necessary to consider the case of several m modes' simultaneous incidence, because the chamber is concentric with the duct and m are independent of each other. Each value of complex amplitudes of the reflected and transmitted waves on each side of the chamber is obtained as follows:

(1) On cross-section 1 in Figure 4, the values of the complex amplitude $P_n^{[A]}$ and $P_s^{[B]}$ are calculated for $P_n^{[in]}$ using equations (18) and (8).

(2) Waves corresponding to $P_s^{[B]}$ are supposed to propagate in the chamber and impinge upon cross-section 2. Then, $P_s^{[C]}$ and $P_n^{[D]}$ are calculated for $P_s^{[B]}$ using equations (22) and (23).

(3) Waves corresponding to $P_s^{[C]}$ are supposed to propagate in the chamber and impinge upon cross-section 1. Then, $P_s^{[E]}$ and $P_n^{[F]}$ are calculated for $P_s^{[C]}$.

(4) Waves corresponding to the summation of $P_s^{[B]}$ obtained in step (1) and $P_s^{[E]}$ obtained in step (3) are supposed to propagate in the chamber and imping upon cross-section 2. Then, $P_s^{[C]}$ and $P_n^{[D]}$ are calculated for $P_s^{[B]} + P_s^{[E]}$.

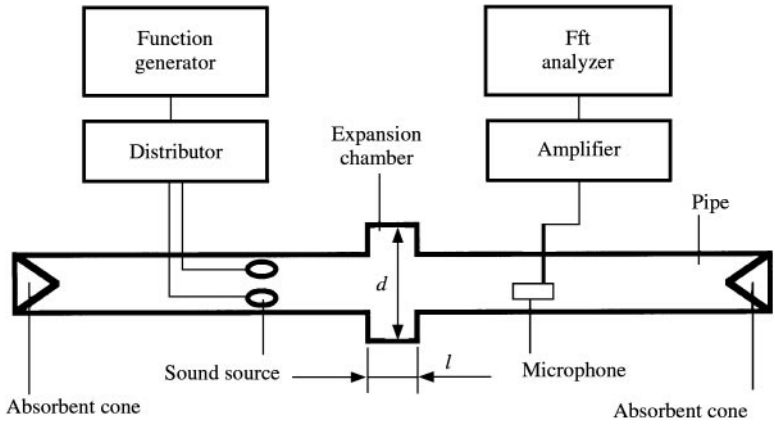

Figure 5. Experimental apparatus.

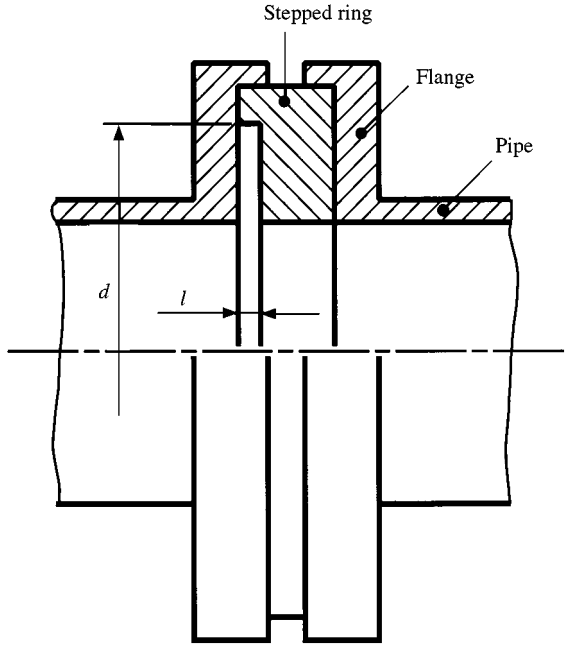

Figure 6. Formation of an extremely short chamber.

(5) Steps (3) and (4) are repeated as follows: for $P_s^{[C]}$ obtained in step (4), $P_s^{[E]}$ and $P_n^{[F]}$ are calculated by step (3); for this $P_s^{[E]}$ and $P_s^{[B]}$ obtained in step (1), $P_s^{[C]}$ and $P_n^{[D]}$ are calculated by step (4).

(6) If the values of $P_n^{[A]} + P_n^{[F]}$ and $P_n^{[D]}$ are converged in the repetition of step (5), this calculation procedure is stopped.

In the above process, it must be considered that each wave's sound pressure changes depending on the chamber length l. For this reason, every calculated value of $P_s^{[B]}$, $P_s^{[C]}$ and $P_s^{[E]}$ is multiplied by $\exp(-j\omega l/v_s)$, which corresponds to the phase change or attenuation of the propagating or non-propagating s-order mode wave respectively.

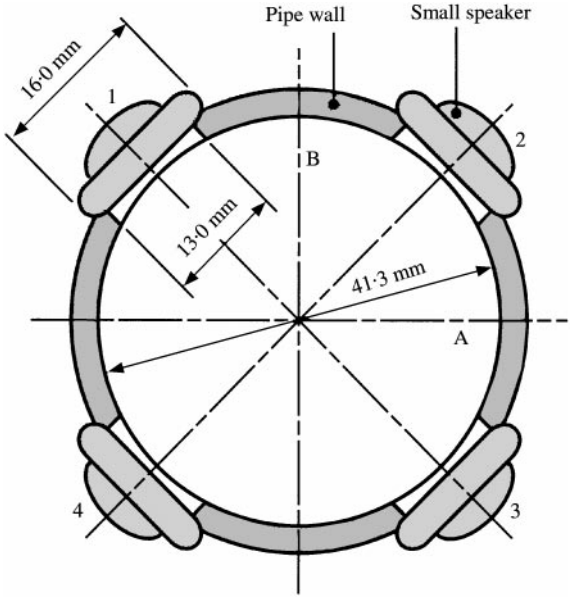

Figure 7. Sound source.

3. VERIFICATION OF CALCULATION BY EXPERIMENT

In order to verify the calculated results, the transmission coefficients are measured with the apparatus shown in Figure 5. The duct comprises two steel pipes with inner diameter $D = 41{\cdot}3$ mm. Each of them has a flange at one end. Between these two flanges, a steel ring or a short pipe with arbitrary inner diameter d and axial length l is placed concentric with the pipes, in order to form the chamber. To form the extremely short chamber, a stepped ring is placed as shown in Figure 6.

Figure 7 shows the sound source. It consists of four small speakers, which are located on the duct wall at intervals of 90° in the circumferential direction. Every speaker radiates sinusoidal sound waves with the same frequency and same amplitude. Actually speaking, four speakers' properties are different from each other. Therefore, we use variable resistance devices connected with them in series that can control each speaker's amplitude separately. If all speaker are excited in phase, the plane wave is generated in the pipe. If speakers 1 and 2 are excited in phase and 3 and 4 are out of phase with π radian, the (1, 0) mode wave (see Figure 2) is generated, which has a node on diameter A indicated in Figure 7. If speakers 1 and 3 are excited in phase and 2 and 4 are out of phase, the (2, 0) mode wave is generated, which has nodes on diameters A and B. The accuracy of sound fields formed by this sound source was confirmed by preliminary tests. In this paper, however, experimental results with the (2, 0) mode wave incidence are omitted, because the frequency range becomes higher and sufficient data could not be obtained for the present pipe size.

A microphone 5·6 mm in diameter is used as shown in Figure 5, which is supported by a thin rod fitted on the pipe wall. It is traversable to the radial direction of the pipe to measure the radial distribution of sound pressure amplitude.

The procedure for measuring the transmission coefficient is as follows: firstly, the ring (or short pipe), which has the same inner diameter as the pipe and same axial length as the chamber concerned, is placed between two flanges in order to form a straight pipe, and

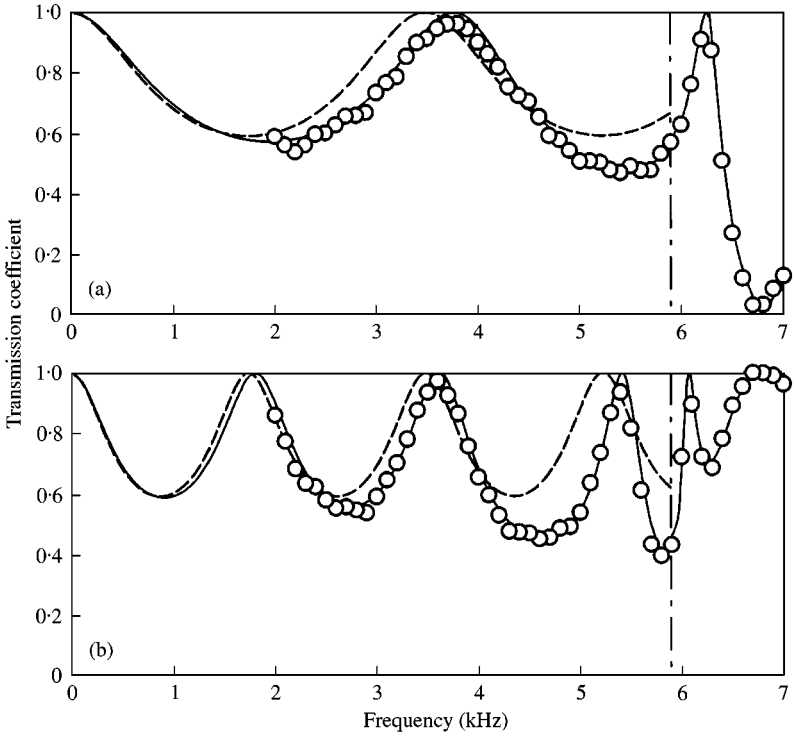

Figure 8. Transmission coefficient at the long chamber with the plane wave incidence, $D = 41{\cdot}3$ mm, $d = 72{\cdot}0$ mm: (a), $l = 50$ mm ($l/d = 0{\cdot}694$); (b), $l = 100$ mm ($l/d = 1{\cdot}39$): ○, measured; ——, calculated by our method; – – –, calculated by the plane wave theory; —·—, (0, 1) cut-off in the chamber.

the amplitude of the sound is measured at an appropriate radial position; after that, the ring (or short pipe) with interested inner diameter d and axial length l is placed, and the amplitude of the sound is measured; the latter amplitude divided by the former amplitude gives the absolute value of the transmission coefficient (amplitude ratio) at the chamber.

With this apparatus, many results were obtained experimentally for comparison with calculated results. Some of them are demonstrated in the following. The temperature was fixed at 25°C in all the experiments. This temperature is applied to all calculations in this paper.

Figure 8 shows the calculated and measured transmission coefficient (versus frequency) at the acoustically long chamber with the plane wave incidence. Conventionally, the transmission coefficient of a long chamber is calculated by

$$\left[1 + \frac{1}{4}\left\{\left(\frac{d}{D}\right)^2 - \left(\frac{D}{d}\right)^2\right\}^2 \sin^2\left(\frac{\omega l}{c}\right)\right]^{-1/2}, \tag{24}$$

which is derived by the plane wave theory. In Figure 8, it is clear that the results using the plane wave theory become incorrect as the frequency becomes high, even in the frequency range where the lowest radial mode (0, 1) is not propagating. Otherwise, our calculated results excellently agree with the measured results, even in the frequency range above the

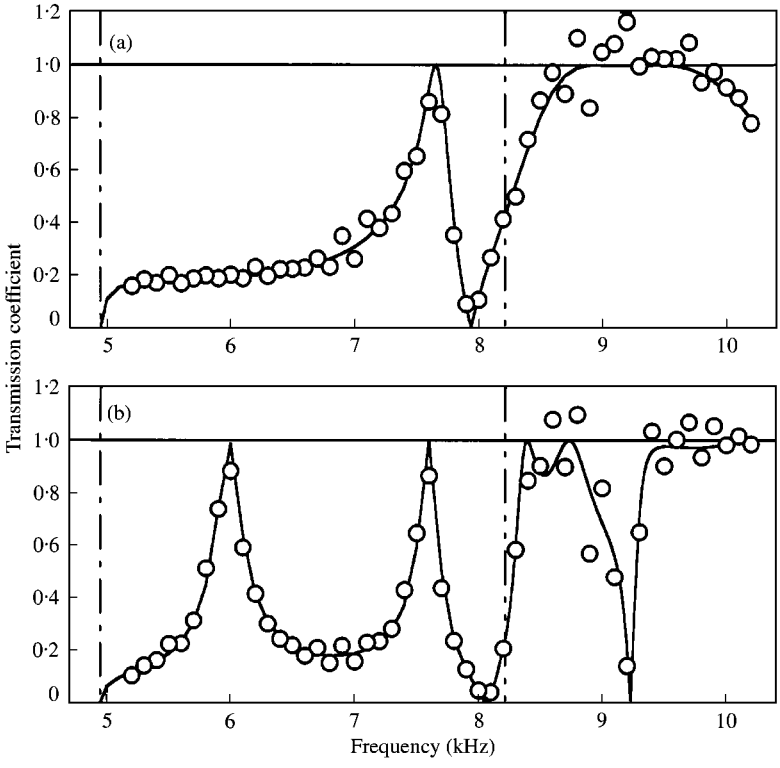

Figure 9. Transmission coefficient at the long chamber with the (1, 0) mode wave incidence, $D = 41{\cdot}3$ mm, $d = 72{\cdot}0$ mm: (a), $l = 50$ mm ($l/d = 0{\cdot}694$); (b), $l = 100$ mm ($l/d = 1{\cdot}39$): ○, measured; ——, calculated; — – —, (1, 0) cut-off in the duct; — - - —, (1, 1) cut-off in the chamber.

(0, 1) cut-off. At the discontinuity of the chamber, not only propagating but also decaying higher mode waves are generated, and cause the dependency of the sound property on the frequency as some researchers had pointed out [2]. In other words, it can be said that our calculation considers enough number of higher modes. Actually, in all cases in this paper, the value of n_1 is fixed at 10 in equation (3).

Figure 9 shows the cases of the (1, 0) mode wave incident to the chamber that has the same geometry as Figure 8. In these cases, the results are obtained in the frequency range where the (1, 0) mode wave can propagate in the duct, i.e., above 4·92 kHz. The agreement between the calculated and measured results is good in the frequency range below the chamber's (1, 1) cut-off. This is one of the evidence to show that our calculation can be applicable to the case of asymmetric mode wave incidence. But in further high frequency range, this agreement becomes somewhat wrong, because the (2, 0) mode wave accidentally generated also becomes cut-on in the duct above 8·16 kHz, and might affect the measured data.

Figure 10 shows the transmission coefficient (versus frequency) at the chamber with the transition length between acoustically long and short. Good agreement between calculated and measured results is obtained in both cases: (a), the plane wave; and (b), the (1, 0) mode wave incidence. Our calculation is considered to be correctly applicable to chambers with such length. In these cases, the transmission property changes remarkably as the chamber length changes. This remarkable change can be explained more in detail using our calculation in section 5.

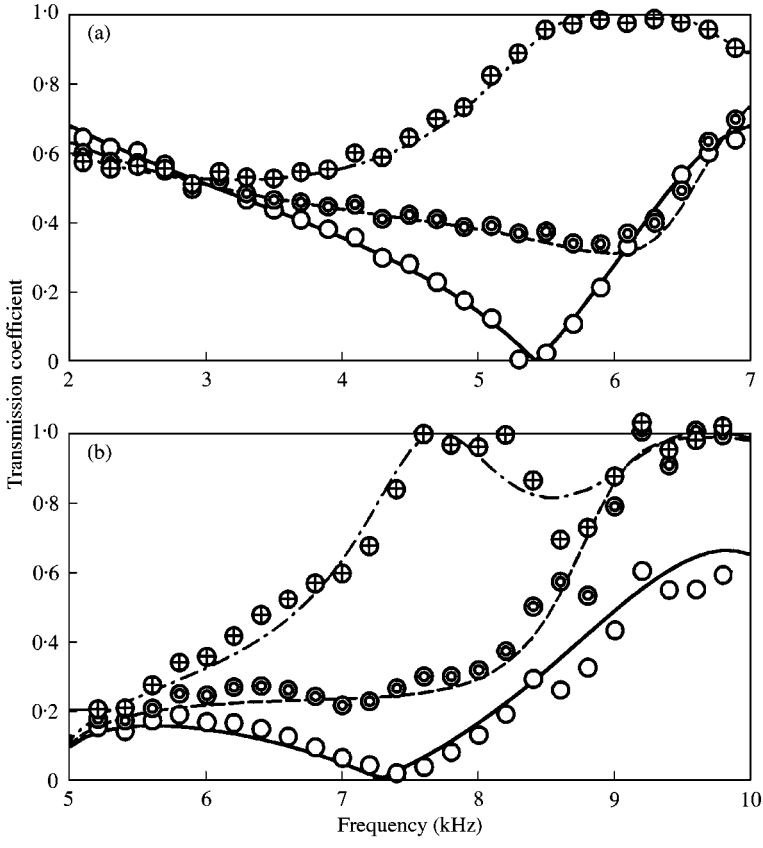

Figure 10. Transmission coefficient at the chamber with transition length: circular marks, measured; curved lines, calculated: (a), the plane wave incidence, $d = 72{\cdot}0$ mm; ○, ——, $l = 25{\cdot}0$ mm ($l/d = 0{\cdot}347$); ●, – – –, 30·0 mm (0·417); ⊕, – – –, 35·0 mm (0·486): (b), the (1,0) mode wave incidence, $d = 66{\cdot}6$ mm; ○, ——, $l = 18{\cdot}0$ mm ($l/d = 0{\cdot}270$); ●, – – –, 22·0 mm (0.330); ⊕, — · —, 26·0 mm (0·390).

4. RESONANT PROPERTIES OF EXTREMELY SHORT CHAMBERS

In this section, we show the results with the extremely short chamber, which resembles a slit on the duct wall as a narrow space between the inlet and outlet sidewall of the chamber. Hence, we call it a "slit" in this section.

Figure 11 shows the measured and calculated transmission coefficient of slits with $D = 41{\cdot}3$ mm and $l = 1{\cdot}0$ mm (i.e. $l/D = 0{\cdot}0242$, and l/d becomes further small as indicated in the caption of Figure 11). In the experimental results in this figure, it can be found that the slit also acts as a resonator muffler. The frequency, where the measured transmission coefficient becomes minimum, which can be called the practical resonant frequency; can be almost correctly predicted by our calculation. However, a remarkable difference appears between the experiment and calculation on the minimum value of the transmission coefficient; i.e., each measured value does not reach zero. This is supposed to be caused by insufficient resonance in a narrow space of the slit. Sound attenuation in a narrow space between two parallel walls is caused mainly by viscosity of air on the wall [16]. Regarding a slit as a side branch of a duct, the sound wave from the duct is realized to propagate from the inlet to the bottom of the branch, then be reflected at the bottom and propagate

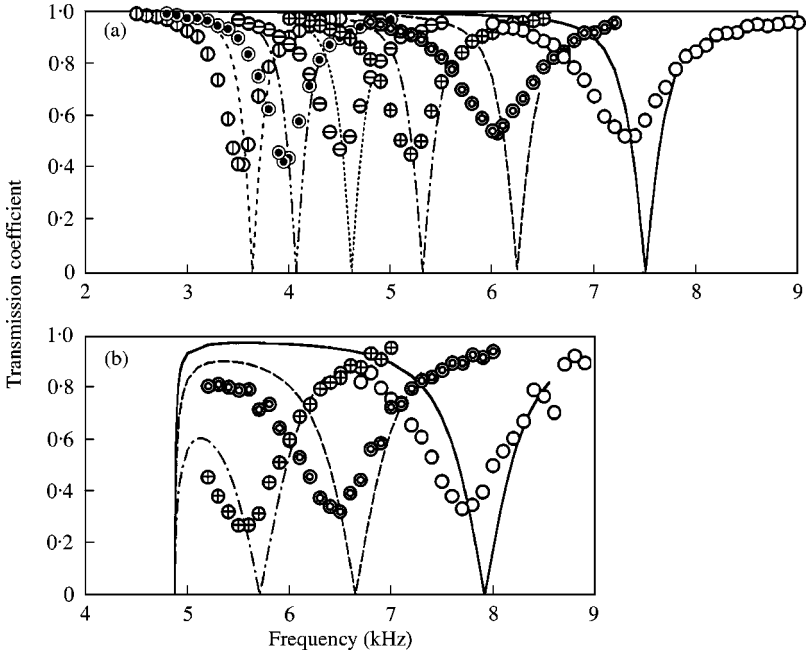

Figure 11. Transmission coefficient at the slit-like chamber, $D = 41{\cdot}3$ mm, $l = 1{\cdot}0$ mm: (a), the plane wave incidence; (b), the (1, 0) mode wave incidence: circular marks, measured; curved lines, calculated: ○, ——, $d = 60{\cdot}0$ mm ($l/d = 0{\cdot}0167$); ●, – – –, 64·0 mm (0·0156); ⊕, – – –, 68·0 mm (0·0147); ⊖, --------, 72·0 mm (0·0139); ◉, — – – —, 76·0 mm (0·0132); ⦶, - - - -, 80·0 mm (0·0125).

from the bottom to the inlet. Such waves would be influenced greatly by viscosity on the wall of the branch.

This consideration mentioned above could be confirmed experimentally with some slits, each of them has several short l. The results are shown in Figure 12, where the following can be found: as l becomes longer, the minimum value of the transmission coefficient approaches 0; the agreement with experiment and calculation becomes better; and this agreement becomes excellent with $l = 5$ mm. This tendency seems to show an evidence of the influence of viscosity. We had presented a simple method to predict actual slit properties regarding the influence of viscosity by modelling the slit as a single-degree-of-freedom system including a damping term [17].

Our attempt in this paper is to show resonant properties of short chambers normalized by various d/D and l/d ratios in section 5. As mentioned above, however, in some cases of the slit, its performance cannot be predicted correctly by our calculation with no regard of the influence of viscosity, which is difficult to treat in our attempt. The reason for this is that on considering the influence of air viscosity on a wall, particle velocity of air would decrease exponentially for the distance from the wall surface along the normal direction. Sound attenuation ratio in narrow space would greatly depend on the width of the space, which correspond not to the l/d ratio but the absolute value of l in the slit case. Therefore, slit properties cannot be normalized by l/d.

Nevertheless, in section 5, we will show short chambers' properties including the slit cases, taking the situation as given below into consideration. If $l/d \ll 1$ but d is sufficiently large, l becomes large enough to be able to ignore the influence of viscosity, and the actual property is expected to be predicted by our calculation. In addition, in the case that l is not

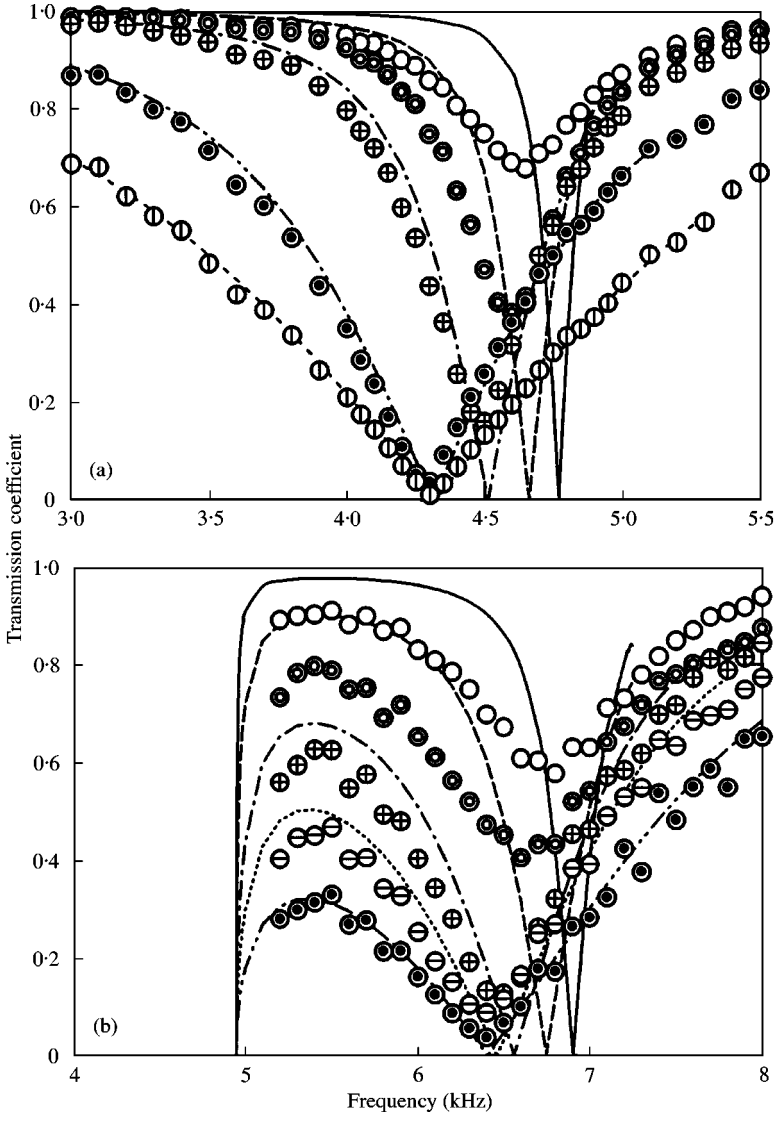

Figure 12. Transmission coefficient at the slit, $D = 41{\cdot}3$ mm: (a), the plane wave incidence, $d = 72{\cdot}0$ mm; (b), the (1, 0) mode wave incidence, $d = 60{\cdot}0$ mm: circular marks, measured; curved lines, calculated: ○, ——, $l = 0{\cdot}5$ mm ●, – – –, 1·0 mm ⊕, – – –, 2·0 mm ⊖, --------, 3·0 mm; ◉, — · – · —, 5·0 mm; ⏀ , - - - -, 10·0 mm.

large, the resonant frequency, which is the most important property of a resonator muffler, can be predicted almost accurately even in the case of extremely short l as shown in Figures 11 and 12.

In this section, the traditional analytical approach, which is based on the summation of sound waves (including decaying modes) in the z direction as a distributed-parameter system, is applied to the slit as an extremely short acoustical element; e.g., the element length becomes $\frac{1}{100}$ of the sound wavelength for $l = 1$ mm slit with 3·4 kHz plane wave incidence. Such a drastic application might not have been taken up by former researchers. In practice, a higher order mode wave is realized as the summation of the plane waves: each of them propagates inclining to the radial or circumferential direction. Hence, our approach is

appropriate to be applied to the slit under the condition that sufficient number of radial modes is taken into account. When the influence of viscosity becomes negligible, our approach seems to be applicable whatever l/D is.

5. COMPREHENSIVE DESCRIPTION OF RESONANT PROPERTIES

In this section, resonant properties of short expansion chambers are comprehensively described using our calculation. In all cases in this section, the size of the chamber is normalized by the ratio of D, d and l.

5.1. THE PLANE WAVE INCIDENCE CASE

In this section, resonant properties are considered with the plane wave incident to the short chamber. For reference, some examples of calculated transmission coefficient curves in the frequency domain are shown in Figure 13: (a), a shallow case; (b), a moderate case; and (c), a relatively deep case. The frequency is normalized by the chamber diameter as $kd/2$, where k is the wavenumber of sound in free space. In these figures, curves of $l/d < 0{\cdot}2$ are not included in order to prevent each figure from becoming complicated to display. In such narrow cases of $l/d < 0{\cdot}2$, every curve becomes analogous with the one shown in Figure 12(a); i.e., the transmission coefficient drops only near the resonant frequency and the sharpness of the curve becomes wider as l/d becomes larger. Generally speaking, the effective frequency range for sound attenuation becomes wider, when l/d and d/D become larger.

In these figures, the frequency where the transmission coefficient reaches zero can be found as the resonant frequency. Although in some cases, e.g., the case of $l/d = 0{\cdot}3$ in (c), more than one resonant frequency is obtained, our attention is directed to the lowest one as a fundamental one. In the case of $l/d > 0{\cdot}4$ in (b) and (c), the minimum transmission coefficient obtained near the fundamental resonant frequency does not reach zero, and it can be said that the resonant frequency disappears. The upper limit length of the resonant-type chamber can be judged as the length where the resonant frequency just disappears. If the length becomes still longer, the property of the chamber in the frequency range below the chamber's (0, 1) cut-off approaches a common expansion-chamber muffler's one as shown in Figure 8.

Many calculations same as in Figure 13 were executed repeatedly, changing the values of d/D and l/d. As the collective result of them, in Figure 14, the relation between the resonant frequency and the chamber length is shown. Both parameters are normalized by the chamber diameter d, as $k_R d/2$ and l/d, where k_R is the wavenumber of sound in free space at the fundamental resonant frequency as explained in Figure 13, and $d/2$ is the chamber radius. In every curve with each d/D, the values with $l/d > 0{\cdot}01$ are plotted. In the cases of $d/D \geqslant 1{\cdot}5$, each curve has the end at $l/d \approx 0{\cdot}4$ that corresponds to the upper limit length of the resonant-type chamber as explained in the previous paragraph using Figure 13.

On surveying Figure 14 roughly, the upper limit length seems to be obtained close to $l/d = 0{\cdot}4$, where the value of $k_R d/2$ approaches 4 regardless of d/D. As mentioned in section 1, it can be generally concluded that the chamber acts as a resonator when $l/d < 0{\cdot}41$ in the plane wave incidence case. This value of 0·41 is obtained by two conditions as follows [3]: $k_R d/2 = 3{\cdot}83$ that corresponds to the chamber's (0, 1) cut-off; and $l = 0{\cdot}5\lambda_R$, where λ_R is the wavelength of the plane wave at the resonant frequency. These conditions can be said to be almost correct in Figure 14, and it can be roughly concluded that the

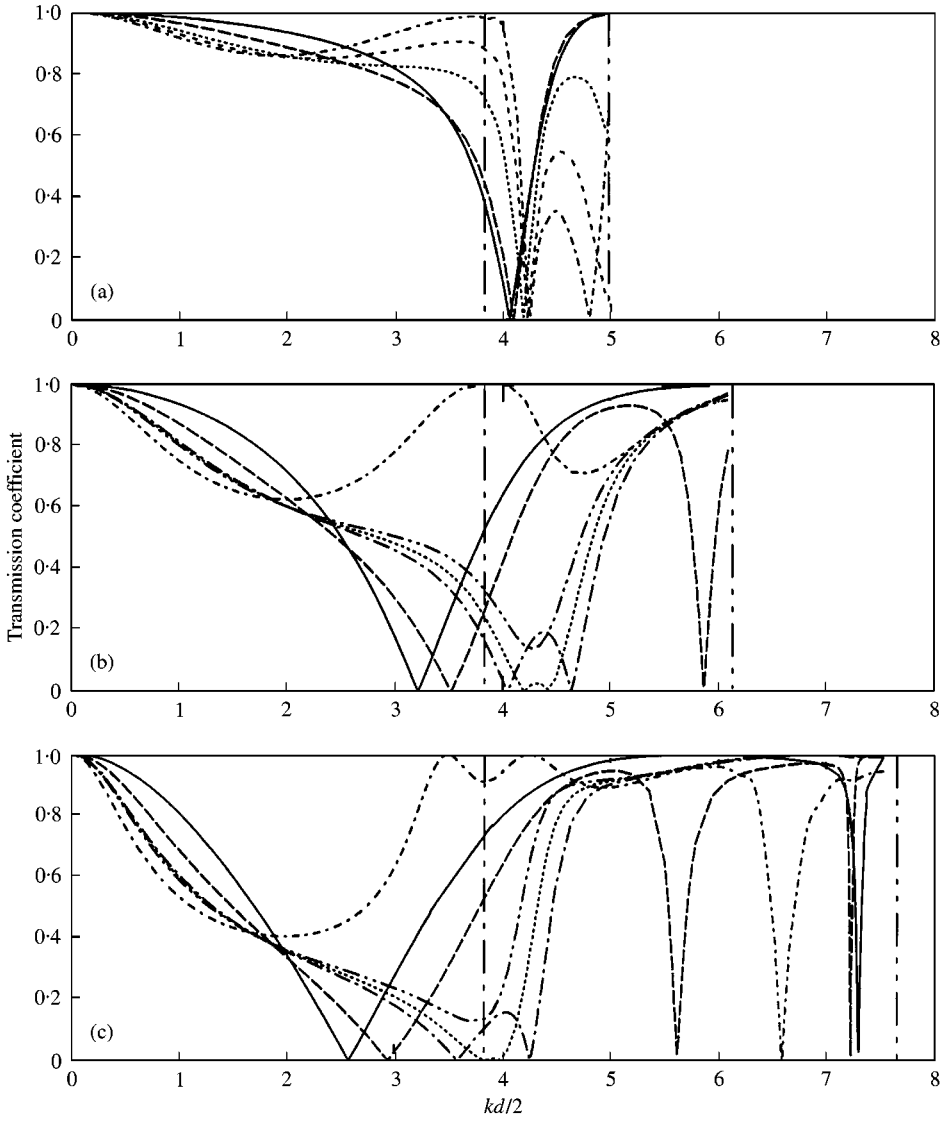

Figure 13. Calculated transmission coefficient versus relative frequency, the plane wave incidence: (a), $d/D = 1{\cdot}3$; (b), 1·6; (c), 2·0: ——, $l/d = 0{\cdot}2$; – – –, 0·3; — · —, 0·39; --------, 0·4; — – —, 0·41; - - - -, 0·45; – – – – – –, 0·5: — · —, (0, 1) cut-off in the chamber; — · · —, (0, 1) cut-off in the duct.

resonant property of the short chamber with upper limit length almost depends on only its diameter regardless of the duct diameter.

If Figure 14 is observed carefully, however, each upper limit of l/d is slightly different depending on d/D. Especially, in the cases of shallow chambers with $d/D = 1{\cdot}3$ and 1·4, no limits are found. In cases of $l/d \geqslant 1{\cdot}5$, as shown in Figures 13(b) and 13(c), a second resonant frequency appears in the frequency range above the chamber's (0, 1) cut-off, and the first and second resonant frequency come close to each other as l/d becomes larger. As generally known, π radian phase shift occurs at the resonant frequency on a simple vibration system with no damping factor. It is supposed that the reason why the resonant frequency disappears near $l/d = 0{\cdot}4$ is that the phase shift is cancelled as $\pi + \pi = 2\pi$, when the first

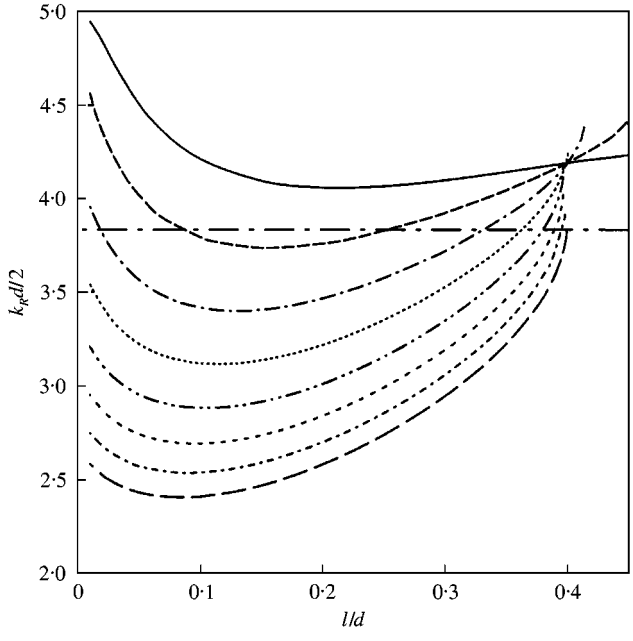

Figure 14. Resonant frequency versus length of short chamber, normalized by chamber diameter, the plane wave incidence: ——, $d/D = 1{\cdot}3$; – – –, 1·4; — · —, 1·5; -----, 1·6; — – – —, 1·7; - - - -, 1·8; - - - - -, 1·9; ——, 2·0; — · —, (0,1) cut-off in the chamber (= 3·83).

resonant frequency meets the second one. On the other hand, in Figure 13(a), every first resonant frequency appears at the range above the chamber's (0, 1) cut-off, and there might be no chance that the second resonant frequency appears, which could cancel the resonant phenomena. This might be the reason why there is no upper limit; in other words, we could not find the decisive transition length between acoustically short and long, in the shallow chamber case. Even in such shallow cases, when l/d becomes long enough, repeating domes as in Figure 8 appear in the range below the chamber's (0, 1) cut-off.

In addition, in Figure 14, the values of each $k_R d/2$ at $l/d \approx 0{\cdot}4$ are found to be slightly different from each other depending on each d/D. The pressure distribution of the (0, 1) mode in the radial direction with diameter d is uniquely decided by d as shown in Figure 2, and the relation between the nodal circle of the (0, 1) mode and the duct outer circle (duct wall) changes following the d/D ratio. Therefore, it must be reasonable that the values of $k_R d/2$ are not perfectly constant regardless of d/D.

In Figure 15, same values as in Figure 14 are plotted as normalized by the chamber depth b, as $k_R b$ and l/b. When d/D is fixed, b/D is also decide uniquely as indicated in the caption of Figure 15. In this figure, it is found that the values of $k_R b$ become almost constant at nearly 1·3 as l/b approaches 0 regardless of d/D except in the case of $d/D = 1{\cdot}3$. This means that the resonant frequency of an extremely short chamber depends on only its depth. Suppose $k_R b = 1{\cdot}3$, b becomes $1{\cdot}3/k_R = 1{\cdot}3\lambda_R/(2\pi) \approx 0{\cdot}21\ \lambda_R$, which means that the chamber depth is a little shorter than the quarter of wavelength of the plane wave. This can be understood as compared with a closed-tube-like side-branch silencer, of whose resonant frequency is obtained when the quarter of wavelength corresponds to its length with an added open-end correction.

In Figure 15, it is clear that $k_R b$ decreases considerably when l/b increases near zero. This might be an evidence showing the dependency of the resonant frequency on the chamber

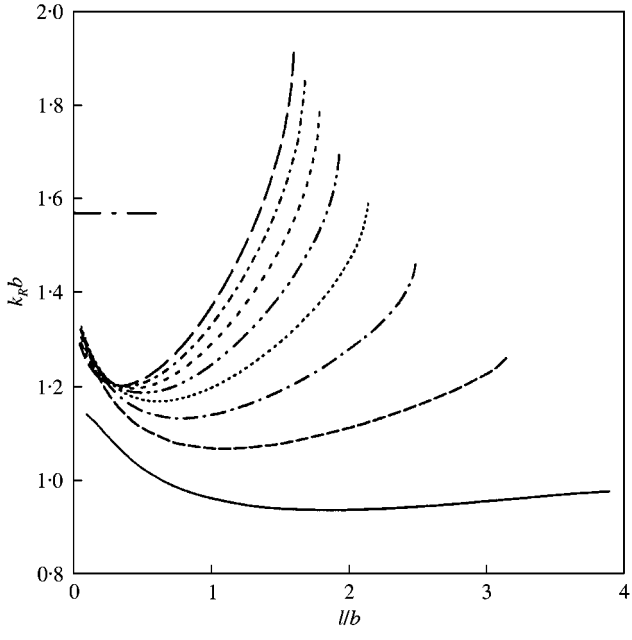

Figure 15. Resonant frequency versus length of short chamber, normalized by chamber depth, the plane wave incidence: ——, $d/D = 1{\cdot}3$ ($b/D = 0{\cdot}15$); – – –, 1·4 (0·2); — · —, 1·5 (0·25); -----, 1·6 (0·3); — · · —, 1·7 (0·35); · · · ·, 1·8 (0·4); – – – – –, 1·9 (0·45); ——, 2·0 (0·5): — · —, $\pi/2$.

depth when l/b is small, in the interpretation that the decrease of the resonant frequency belonging to the increase of l is realized as the increase of the corresponding open-end correction. When l/b becomes wider to some extent, then the resonant frequency begins to increase to approach the upper end value of $k_R d/2 \approx 4$ as shown in Figure 14.

In Figures 14 and 15, results are not shown in the case of $d/D < 1{\cdot}3$ ($b/D < 0{\cdot}15$). The resonant frequency of such a shallow chamber becomes higher and exceeds the duct's (0, 1) cut-off frequency. In this frequency range, when even only the plane wave propagates to the chamber, the (0, 1) mode wave can be radiated at the chamber and starts to propagate in the duct together with the plane wave, and transmission properties become complex such that they cannot be included easily in Figures 14 and 15. Even in the case of $d/D = 1{\cdot}3$, as supposed with Figure 14, the resonant frequency is likely to exceed the duct's (0, 1) cut-off (where $k_R d/2 = 3{\cdot}83 \times 1{\cdot}3 \approx 4{\cdot}98$, $k_R b = 3{\cdot}83 \times 0{\cdot}3 \approx 1{\cdot}15$), when l approaches zero. In this case, assuming $k_R b = 1{\cdot}3$ against Figure 15, $k_R D/2$ becomes $1{\cdot}3/0{\cdot}3 \approx 4{\cdot}33$ that exceeds the duct's (0, 1) cut-off ($kD/2 = 3{\cdot}83$). Judging from this, the case of $d/D = 1{\cdot}3$ seems to be a critical case, and the value of $k_R b$ near $l/b = 0$ might be different from other d/D cases to some extent in Figure 15.

5.2. ASYMMETRIC MODE WAVE INCIDENCE CASE

In this section, the same procedure as in section 5.1 is developed in order to indicate properties of short chambers with asymmetric mode wave incidence.

For reference, some examples of transmission coefficient curves in the frequency domain are shown in Figure 16 with the (1, 0) mode wave incidence: (a), a shallow case; and (b),

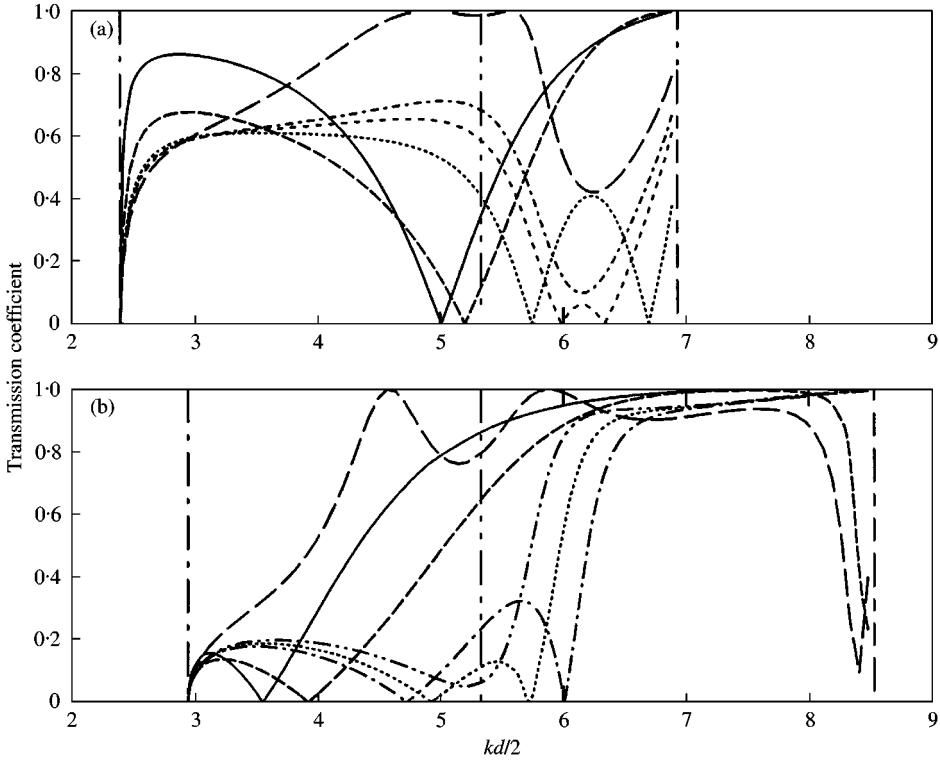

Figure 16. Calculated transmission coefficient versus relative frequency, the (1, 0) mode wave incidence: (a), $d/D = 1{\cdot}3$; (b), 1·6; ——, $l/d = 0{\cdot}1$; – – –, 0·2; — - —, 0·29; --------, 0·3; — - - —, 0·31; - - - -, 0·32; – – – – – –, 0·33; — —, 0·4: — - —, (1, 0) cut-off in the duct; — - - —, (1, 1) cut-off in the chamber; - - —, (1, 1) cut-off in the duct.

a relatively deep case. Same as with Figure 13, the frequency is normalized using $kd/2$ parameter. Calculations are carried out in the frequency range between the duct's (1, 0) and (1, 1) cut-off because: below the (1, 0) cut-off, the (1, 0) mode wave cannot propagate in the duct and there is no meaning to consider; above the (1, 1) cut-off, the (1, 1) mode wave starts to propagate together with the (1, 0) mode wave and a transmission coefficient cannot be defined easily. In order to prevent figures becoming complicated, curves of $l/d < 0{\cdot}1$ are not shown, but in such cases, each curve drops only near the resonant frequency as shown in Figure 12(b).

In both figures in Figure 16, remarkable changes of transmission properties occur near $l/d = 0{\cdot}3$, where the transmission curves changes are similar to the plane wave case in Figure 13 as follows: with the increases of l/d, the second resonant frequency appears; two resonant frequencies come close; then the resonance disappears, where it is considered that the chamber has the upper limit length of resonant-type.

Using the same procedure as in Figures 14 and 15, normalized resonant frequencies are shown in Figures 17 and 18 with the (1, 0) or the (2, 0) mode wave incidence respectively. The range of d/D is limited within 1·3–1·6 for Figure 17, and 1·3–1·4 for Figure 18, in order to exclude two cases as follows: if a shallow chamber ($d/D < 1{\cdot}3$) is considered, the resonant frequency exceeds the duct's (1, 1) or (2, 1) cut-off, and resonant properties become complicated; if a deep chamber ($d/D > 1{\cdot}6$ for Figure 17, and 1·4 for Figure 18) is considered, the resonant frequency tends to be less than the duct's (1, 0) or (2, 0) cut-off and disappears, as supposed in Figure 16(b).

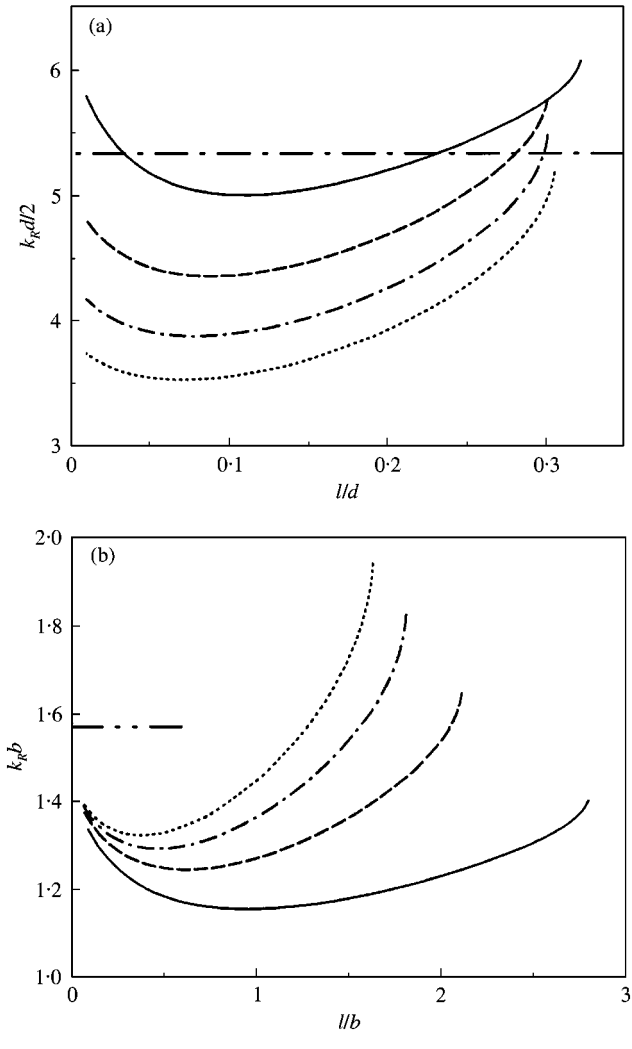

Figure 17. Resonant frequency versus length of short chamber, the (1, 0) mode wave incidence: (a), normalized by chamber diameter; (b), normalized by the chamber depth: ——, $d/D = 1{\cdot}3$; – – –, 1·4; — · —, 1·5; ·····, 1·6: — · · —, (1, 1) cut-off in the chamber (= 5·33); — – – —, $\pi/2$.

With a rough survey of Figure 17(a), the upper limit length of a resonant-type chamber is obtained at $l/d \approx 0{\cdot}3$, where each normalized resonant frequency $k_R d/2$ with each d/D comes near 5·33 that is the chamber's (1, 1) cut-off. This can be considered following two conditions, which belong to an extended interpretation from the plane wave case mentioned in section 5.1: the chamber length l is the half of the incident (m, n) mode's wavelength; and the $(m, n + 1)$ mode becomes cut-on in the chamber. Namely,

$$l = \lambda_{mn}/2 = \pi v_{mn}/\omega = \pi c/(\omega^2 - \omega_{mn}^2)^{1/2}, \tag{25}$$

$$\omega_{mn+1} = 2q_{mn+1}\, c/d, \tag{26}$$

where λ_{mn} is the wavelength in the z direction of the (m, n) mode wave. By substituting $\omega = \omega_{mn+1}$ into equation (25), and eliminating c from two equations,

$$l/d = \pi/\{2\,(q_{mn+1}^2 - q_{mn}^2)^{1/2}\} \tag{27}$$

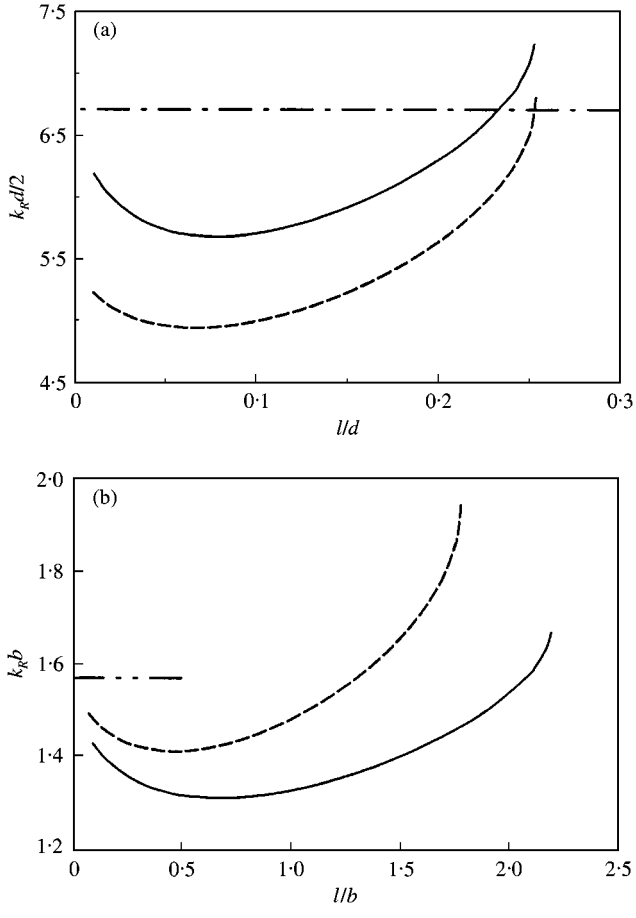

Figure 18. Resonant frequency versus length of short chamber, the (2, 0) mode wave incidence: (a), normalized by chamber diameter; (b), normalized by the chamber depth: ——, $d/D = 1{\cdot}3$; – – –, 1·4; — · —, (2, 1) cut-off in the chamber (= 6·71); — · · —, $\pi/2$.

is obtained. By substituting $q_{10} = 1{\cdot}84$ and $q_{11} = 5{\cdot}33$ into equation (27), $l/d = 0{\cdot}314$ is obtained for the (1, 0) mode wave incidence. This l/d value moderately agrees with the upper end of each curve in Figure 17(a).

On the other hand, in Figure 17(b), each curve with each d/D concentrates to $k_R b \approx 1{\cdot}4$ as l/b approaches 0. This is realized with the same interpretation as in section 5.1. Although the values of $k_R b$ are slightly larger than the values of the plane wave incidence case in Figure 15, it is supposed that the extremely short chamber acts as a side-branch silencer and depends on the wavelength of the plane wave with non-plane mode wave incidence.

The same consideration and interpretation mentioned above are applicable to Figure 18 for the (2, 0) mode wave incidence case. By substituting $q_{20} = 3{\cdot}05$ and $q_{21} = 6{\cdot}71$ into equation (27), $l/d = 0{\cdot}263$ is obtained. Close to this l/d in Figure 18(a), the upper limit of a resonant-type chamber is obtained, and $k_R d/2$ approaches nearly 6·71 corresponding to the chamber's (2, 1) cut-off. On the other hand, in Figure 18(b), both curves with each d/D approach $k_R b \approx 1{\cdot}5$ as l/b approaches 0. Although the values of $k_R b$ are slightly larger than the values of the (1, 0) mode wave incidence case in Figure 17(b), the condition in which the depth of the chamber is slightly shorter than the quarter of wavelength of the plane wave at the resonant frequency is maintained.

6. CONCLUSIONS

In this paper, resonant properties of short expansion chambers are studied comprehensively using the traditional analytical approach treating a duct system as a distributed-parameter system. With the development of the analytical approach with simply refined equations and containing enough number of radial modes in calculation, not only the cases of moderately short chambers and the plane wave incidence but also the cases that include extremely short chambers and/or asymmetric mode wave incidence are investigated. The results are verified experimentally with the apparatus that can radiate the plane wave and asymmetric mode waves in a duct. In almost all the cases, the measured and calculated transmission coefficients coincide excellently. The applicability of our approach to various cases of short chambers is confirmed.

In a duct system with a simple concentric expansion chamber, with no regard of viscosity, linear acoustic fields are decisively described by the duct diameter, the chamber diameter and the chamber length with the relative frequency. We denote the chamber's property normalized by the ratio of the duct and chamber diameter, and the ratio of the chamber length and diameter. Using these normalizations, as general results of this research, the following is found:

(1) In almost all the cases, the transition length of an expansion chamber between acoustically short (resonant-type) and long (represented by the repeating done-shaped transmission loss curve) depends on two conditions as follows: the chamber length becomes half of axial wavelength of the incident (m, n) mode; and the $(m, n + 1)$ mode becomes cut-on in the chamber. These two conditions are confirmed with various dimensions of chambers and with asymmetric mode wave incidence. In other words, with the upper limit length (transition length) of a resonant-type chamber, the resonant frequency of the chamber almost depends on only the chamber diameter regardless of the duct diameter and with any mode wave incidence.

(2) In the case of an extremely short chamber, which resembles a slit on the duct wall, the resonant frequency is almost correctly normalized by the chamber depth and the wavelength of the plane wave, regardless of other dimensions and with any mode wave incidence. This property is realized in comparison with a side-branch silencer with an open-end correction. For practical application, such a chamber might be expected to work as a resonator muffler, which can be applicable in a very narrow axial space.

(3) In all cases of resonant-type chambers with any mode wave incidence, as the chamber length increases form extremely short to relatively long, the resonant frequency firstly decreases from the value mentioned in (2); then increases to approach the value mentioned in (1).

REFERENCES

1. A. I. EL-SHARKAWY and A. H. NAYFEH 1978 *Journal of the Acoustical Society of America* **63**, 667–674. Effect of an expansion chamber on the propagation of sound in circular ducts.
2. A. SELAMET and P. M. RADAVICH 1997 *Journal of Sound and Vibration* **201**, 407–426. The effect of length on the acoustic attenuation performance of concentric expansion chambers: an analytical, computational and experimental investigation.
3. J. W. SULLIVAN and M. J. CROCKER 1978 *Journal of the Acoustical Society of America* **64**, 207–215. Analysis of concentric-tube resonators having unpartitioned cavities.
4. For example, J. IH and B. LEE 1985 *Journal of the Acoustical Society of America* **77**, 1377–1388. Analysis of higher-order mode effects in the circular expansion chamber with mean flow.
5. P. V. KUZNETSOV and G. S. NOSKO 1984 *Soviet Physics-Acoustics* **30**, 223. Sound attenuation in a wide cylindrical tube with annular grooves in the wall.

6. For example, A. SELAMET and Z. L. JI 2000 *Journal of Sound and Vibration* **229**, 3–19. Acoustic attenuation performance of circular expansion chambers with single-inlet and double-outlet.
7. J. MILES 1944 *Journal of the Acoustical Society of America* **16**, 14–19. The reflection of sound due to a change in cross section of a circular tube.
8. M. L. MUNJAL 1987 *Acoustics of Ducts and Mufflers*. New York: John Wiley.
9. J. M. TYLER and T. G. SOFRIN 1961 *S. A. E. Transaction* **70**, 309–332. Axial flow compressor noise studies.
10. A. SADAMOTO, Y. MURAKAMI and S. MASUDA 1993 *Transactions of the Japan Society of Mechanical Engineers* (Series C) **59**, 3860–3865. Attenuation of sound including higher-order mode waves in circular duct using a narrow slit on the duct wall (in Japanese).
11. A. SADAMOTO and Y. MURAKAMI 1995 *Transactions of the Japan Society of Mechanical Engineers* (Series C) **61**, 1484–1489. Effects of expansion-chamber muffler on high-frequency sounds in circular duct (in Japanese).
12. A. SADAMOTO and Y. MURAKAMI 1996 *Transactions of the Japan Society of Mechanical Engineers* (Series C) **62**, 110–115. Properties of expansion-chamber muffler with short axial length (in Japanese).
13. R. J. ALFREDSON 1972 *Journal of Sound Vibration* **23**, 433–442. The propagation of sound in a circular duct of continuously varying cross-sectional area.
14. L. J. ERIKSSON 1980 *Journal of the Acoustical Society of America* **68**, 545–550. Higher order mode effects in circular ducts and expansion chambers.
15. H. HUDDE and U. LETENS 1985 *Journal of the Acoustical Society of America* **78**, 1826–1837. Scattering matrix of a discontinuity with a nonrigid wall in a lossless circular duct.
16. A. CUMMINGS 1993 *Journal of Sound and Vibration* **162**, 27–42. Sound propagation in narrow tubes of arbitrary cross-section.
17. A. SADAMOTO and Y. MURAKAMI 1998 *Transactions of the Japan Society of Mechanical Engineers* (Series C) **64**, 1985–1990. Quantitative estimate of sound attenuation of a slit-like duct expansion considering sound damping in it (in Japanese).